A self-consistent analysis of a collisional presheath

Monojoy Goswami and H. Ramachandran

Citation: Physics of Plasmas (1994-present) **6**, 4522 (1999); doi: 10.1063/1.873739
View online: http://dx.doi.org/10.1063/1.873739
View Table of Contents: http://scitation.aip.org/content/aip/journal/pop/6/12?ver=pdfcov
Published by the AIP Publishing

A self-consistent analysis of a collisional presheath

Monojoy Goswami[a] and H. Ramachandran
Institute for Plasma Research, Bhat, Gandhinagar 382 428, Gujarat, India

(Received 25 June 1999; accepted 13 September 1999)

A one-dimensional plasma discharge is analyzed under steady state conditions. Using simple models for source and collisions, a first-order differential equation is obtained that simultaneously describes both the bulk and the presheath of the plasma. This equation is numerically solved in various regimes and physically interesting quantities such as the ratio of bulk to edge density and the size of the inertial terms in the bulk region are presented. Analytic expressions are obtained for profiles when collision frequency is assumed constant. Findings include $n_B/n_{SE}\sim 2.5$ for highly collisional systems, significant flow in the bulk plasma, and modified $I-V$ characteristics. © *1999 American Institute of Physics.* [S1070-664X(99)04312-8]

I. INTRODUCTION

The theory of sheaths is an old subject[1,2] that has gained considerable recent attention[3,4] due to its importance in the understanding of plasma devices used in plasma processing. These plasma systems are usually very collisional and considerable attention has been paid to the issue of the nature of the Bohm sheath in the presence of sources[4] and collisions.[4–6] Less attention has been paid to the presheath of a plasma and the nature of its connection to the bulk. This is a more elusive problem as it involves the influence of the electrostatic field inside the quasineutral part of the plasma system. However, it is of crucial importance to understanding of physics of this region as it is instrumental in throttling the steady state flow of plasma constituents to the sheath.

Many numerical studies of this problem have of course been done,[7–11] but they suffer uniformly from two limitations. To model the plasma volume, they discretize the spatial co-ordinates in steps that usually exceeds λ_{mfp}. This makes it virtually impossible to do justice to the presheath which has structures inside the λ_{mfp} scale. On the other hand, studies that explore the presheath must necessarily terminate at an infinite bulk. The current study is an attempt to do justice to both regimes of the plasma chamber through the use of a simple model that includes collisions on the one hand, and sources on the other. A simple but reasonable collision operator is used that exhibits the correct properties in the bulk ($\nu\sim$constant) and the presheath ($\lambda_{mfp}\sim$constant). The resulting equation is simple enough to be solved accurately for a system hundreds of λ_{mfp} long, yet retains all the physics of presheath dynamics.

The interesting special case of a system with $\nu\sim$constant everywhere is also treated. This problem is analytically tractable and solutions are presented. Such a treatment is appropriate when Coulomb collisions dominate neutral collisions, since ions can only slow down against electrons, and ν_{ie} is velocity independent. However, such systems are not to be found in practice even in tokamak edge plasmas, and the treatment is included here mainly for its value in interpreting the numerical study.

$I-V$ characteristics are obtained for a discharge with equal sized anode and cathode. (The more general case is equally simple to do, but the authors choose to restrict the phase space of parameters and keep the treatment as simple as possible). The results have been compared with the two conventional limits of ambipolar theory[12] and ideal presheath theory,[13] as well as the ν=constant solution developed in this paper. Excellent agreement is obtained in all limits.

The application of fluid equations for the ions in the presheath, especially near the sheath edge, may be questioned. However, fluid theory has been successfully used in a variety of treatments of the plasma presheath (Ref. 14, and references therein). Chodura[15,16] has applied fluid theory to the plasma presheath for the case of a cold ion source. In these applications it was assumed that the collisional mean free path of the plasma particles is short enough that a fluid description was sufficient. Kino and Shaw[17] have shown that fluid theory can adequately describe the plasma presheath in the collisionless limit. This treatment, however, also assumed the ions to be born cold. Scheuer and Emmert[14] have shown that the fluid equations may be applied to presheath, with reasonable results, to cases in which the mean free path is both long and short compared to the plasma dimensions with a source of warm ions. Although there are some differences between the fluid and kinetic results, the fluid approximation appears to be a reasonable approach to calculating presheath profiles along with the bulk plasma.

The organization of the paper is as follows: Section II introduces the geometry of the model and obtains the equations; Sec. III discusses the numerical techniques followed in the solution of the equations; Sec. IV analytically solves the ν=constant model; and Sec. V presents the results with the discussion. Appendix A contains the derivation of the collision operator used; Appendix B presents briefly the ambipolar equations in the notation of this paper for reference; and Appendix C presents small velocity perturbative solutions of the equations used in the numerical procedure to integrate through an internal singular point.

[a]Electronic mail: monojoy@plasma.ernet.in

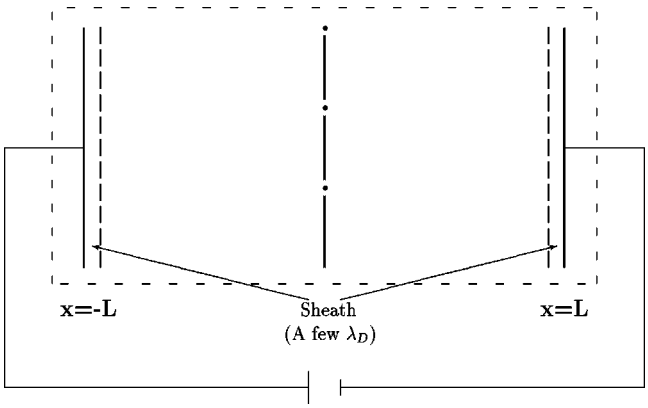

FIG. 1. Schematic of the model system.

II. MODEL EQUATIONS

The model system under consideration is shown in Fig. 1. A plasma consisting of electrons and singly charged ions is assumed present between two capacitor plates placed at $x=\pm L$. The following assumptions have been used to obtain the model equations derived in this section.

(1) The gas is weakly ionized so that collisions with neutral particles dominate Coulomb collision processes.

(2) The pressure is low enough for a glow discharge to be obtained but high enough to treat the electrons and ions collectively as fluid.

(3) For the purpose of this paper, a uniform, constant source is assumed to be present. In this treatment, the source is *not* assumed to depend on plasma parameters such as the electron density and temperature. This is not realistic, but as the focus of this treatment is on the interaction between bulk and presheath behavior, the source properties have been simplified to make the equations transparent.

(4) The electrons are assumed to be isothermal while ions are assumed to be adiabatic. More important, a single value of γ_i is used for the entire column. This is a major simplification, and its consequence will be explored further in the discussion at the end of the paper.

(5) The ions (assumed singly charged) are assumed to exchange energy rapidly in elastic collisions, and therefore are at the same temperature as the neutral species. This results in a constant ion-acoustic velocity, allowing the equations to be meaningfully normalized.

(6) No magnetic fields are applied.

(7) No negative ions are present.

(8) The walls are assumed to be ideal, i.e., there is no secondary emission from the wall.

(9) The sheath region itself is assumed collisionless and well described by classical Bohm sheath theory. The present treatment focuses on the nature of the presheath that connects this sheath to the collisional bulk.

The above-mentioned assumptions can be easily relaxed, but the increased dimension of the parameter space hinders interpretation.

The time-independent continuity equation for the ions in one dimension is given by

$$\frac{d}{dx}(n_i v_i)=S_0, \tag{1}$$

where n_i and v_i are the density and flow velocity of the ions, respectively. The momentum equation in steady state for particles of species α is

$$m_\alpha n v_\alpha \frac{dv_\alpha}{dx}=q_\alpha n E_x-\frac{dp_\alpha}{dx}-m_\alpha n \nu_\alpha v_\alpha-m_\alpha S_0 v_\alpha, \tag{2}$$

where quasineutrality has been assumed to be valid, i.e., $n_e \approx n_i \approx n$, and viscosity effects have been neglected. An external current I_{ext} is assumed to flow from the anode (at $x=-L$) to the cathode (at $x=+L$). This current is given by

$$I_{\text{ext}}=A j_{\text{ext}}=(v_i-v_e)neA, \tag{3}$$

where A is the total collection area of the electrode, assumed equal for both cathode and anode.

Equation (2) for electrons is

$$0=-enE_x-\frac{dp_e}{dx}-m_e n \nu_e v_e, \tag{4}$$

where only terms of $\mathcal{O}(\sqrt{m_e/m_i})$ have been retained. This amounts to treating the electrons as inertialess. Adding Eq. (4) to Eq. (2) for ions yields

$$m_i n v_i \frac{dv_i}{dx}=-\frac{d}{dx}(p_e+p_i)-m_i n \nu_i v_i\left(1+\frac{m_e \nu_e}{m_i \nu_i}\right)+m_e \nu_e \frac{I_{\text{ext}}}{eA}-m_i S_0 v_i, \tag{5}$$

where Eq. (3) has been used to eliminate v_e. Using the assumption of adiabatic ions and isothermal electrons, the first term on the right-hand side becomes $(T_e+\gamma T_i)dn/dx$. Using Eq. (1) to eliminate dn/dx, Eq. (5) when normalized, yields

$$\frac{dM}{d\xi}-\frac{L\nu_i}{c_s}\frac{M^2\left(1+\frac{m_e\nu_e}{m_i\nu_i}\right)}{1-M^2}=\frac{S_0 L}{n c_s}\left[\frac{1+M^2}{1-M^2}-\frac{m_e}{m_i}\frac{I_{\text{ext}}}{S_0 LeA}\frac{L\nu_e}{c_s}\frac{M}{1-M^2}\right], \tag{6}$$

where $\xi=x/L$ is the normalized position, $M=v_i/c_s$ the Mach number, and $c_s=\sqrt{(T_e+\gamma T_i)/m_i}$ the ion acoustic speed.

Equation (6) includes dissipative effects through the presence of ν_e and ν_i. For the system envisaged here, ν_e and ν_i are the average slowing down times for the electrons and ions. The plasma is assumed to be tenuous enough that collisions with the neutrals dominate. These collisions, when averaged over the distribution, are shown in Appendix A to take the form

$$\frac{L\nu_i}{c_s}=\alpha\sqrt{1+\frac{\pi}{8}\frac{M^2}{\bar{M}^2}}, \quad \frac{L\nu_e}{c_s}=\alpha\sqrt{\frac{m_i}{m_e}\frac{T_e}{T_i}}, \tag{7}$$

where $\alpha=4L\bar{M}/2\pi\lambda_{\text{mfp}}$, λ_{mfp} the mean free path for collisions and $\bar{M}=\sqrt{T_i/(T_e+\gamma T_i)}$ is the thermal velocity

($\sqrt{T_i/m_i}$) of ions normalized to c_s. The velocity dependence in $L\nu_i/c_s$ results in the bulk ions experiencing a constant collision frequency, while the presheath ions experience a constant mean free path. Such a model is essential for any description that seeks to simultaneously model both bulk and presheath physics. Using Eq. (7), Eq. (6) becomes

$$\frac{dM}{d\xi}-\frac{\alpha M^2}{1-M^2}\left[\sqrt{1+\frac{\pi M^2}{8\bar{M}^2}}+\mu\sqrt{\tau}\right]=\frac{S_0L}{nc_s}\left[\frac{1+M^2-2\delta M}{1-M^2}\right], \tag{8}$$

where $\mu=\sqrt{m_e/m_i}$, $\tau=T_e/T_i$, and $\delta=\alpha\mu\sqrt{\tau}\tilde{I}$. $\tilde{I}=I_{\text{ext}}/(eAS_0L)$ is the normalized external current and $\gamma=3$ is the adiabatic constant. Equation (8) has the deficiency that it uses a single γ to describe the entire system. While ions are well described as adiabatic in the sheath and presheath, they are isothermal ($\gamma=1$) on the transport time scales that occur in the bulk. This matter is taken up again in Sec. V when the results are discussed.

Equation (8) may be converted into an equation purely for M, by making use of Eq. (1). Since Eq. (8) must satisfy

$$M=\pm 1$$

at

$$\xi=\pm 1 \tag{9}$$

as required by the Bohm sheath, M must become zero for some ξ_0, $-1<\xi_0<1$. This yields an initial condition for Eq. (1), namely, $n(\xi_0)M(\xi_0)=0$. Using the assumption of a constant S_0, Eq. (1) is then solved to obtain

$$\frac{S_0L}{nc_s}=\frac{M}{\xi-\xi_0}. \tag{10}$$

Hence Eq. (8) becomes

$$\frac{dM}{d\xi}-\frac{\alpha M^2}{1-M^2}\left[\sqrt{1+\frac{\pi M^2}{8\bar{M}^2}}+\mu\sqrt{\tau}\right]=\frac{M}{\xi-\xi_0}\left[\frac{1+M^2-2\delta M}{1-M^2}\right]. \tag{11}$$

The need for two boundary conditions is now clear: Equation (11) is an eigenvalue problem and has solutions only for specific ξ_0. Equation (11) has coefficients that are singular both at $\xi=\pm 1$ and at $\xi=\xi_0$. The singularity at $\xi=\xi_0$ is intrinsic, but the singularity at $\xi=\pm 1$ may be removed by solving for ξ as a function of M:

$$\frac{d\xi}{dM}=\frac{1-M^2}{M}\frac{\xi-\xi_0}{\alpha M(\xi-\xi_0)\left[\sqrt{1+\frac{\pi}{8}\frac{M^2}{\bar{M}^2}}+\mu\sqrt{\tau}\right]+(1+M^2-2\delta M)} \tag{12}$$

with $\xi=\pm 1$ at $M=\pm 1$ and $\xi\to\xi_0$ as $M\to 0$.

The characteristic feature of Eq. (11) is that it captures the physics of bulk and presheath in a single equation. When $\lambda_{\text{mfp}}\gg L$, i.e., $\alpha\to 0$, Eq. (12) reduces to conventional presheath equation[13]

$$\frac{dM}{d\xi}=\frac{M}{\xi-\xi_0}\left[\frac{1+M^2}{1-M^2}\right]. \tag{13}$$

The ambipolar limit of Eq. (12) can be obtained by assuming $\lambda_{\text{mfp}}\ll L$ and $M\ll\bar{M}$. This refers to a plasma dominated by diffusive processes, where necessarily the mean free path is small and the flow velocities are small compared to thermal velocities of the species. With these assumptions Eq. (11) reduces to

$$\frac{dM}{d\xi}-\alpha M^2(1+\mu\sqrt{\tau})=\frac{M}{\xi-\xi_0}(1-2\delta M). \tag{14}$$

Using Eq. (1) to substitute for $dM/d\xi$, and assuming zero current ($\delta=0$), this yields

$$-\frac{1}{\alpha(1+\mu\sqrt{\tau})}\frac{d^2n}{d\xi^2}=1, \tag{15}$$

which is the normalized ambipolar diffusion equation as subsequently shown by Eqs. (B3) and (B4).

Equations (10) and (12) completely specify the plasma equilibrium for given L/λ_D and I_0/S_0LeA. Particle conservation clearly requires $2S_0L=(n(-1)+n(+1))c_s$, which yields the proper normalization for density: $\tilde{n}=2n/(n(1)+n(-1))$. To obtain $I-V$ characteristics, the potential difference developed across the system is also required. The applied potential $\Delta\Psi=(\Psi_A-\Psi_C)$ may be split into three parts:

$$\Delta\Psi=[\Psi_A-\Psi(-1)]+[\Psi(-1)-\Psi(+1)]+[\Psi(+1)-\Psi_C], \tag{16}$$

where Ψ's are potentials normalized to T_e/e and Ψ_A and Ψ_C are the normalized potentials at the anode and cathode, respectively. Following the standard treatment[4] of Bohm sheaths,

$$\tilde{I}=\tilde{n}(1)-\tilde{\Gamma}_e(1)=\tilde{n}(1)-M_{e+}\tilde{n}(1)\exp(-(\Psi(1)-\Psi_C)),$$

i.e.,

$$\Psi_C-\Psi(1)=\ln\left[\frac{1-\tilde{I}/\tilde{n}(1)}{M_{e+}}\right] \tag{17}$$

and

$$\tilde{I} = -\tilde{n}(-1) - \tilde{\Gamma}_e(-1)$$
$$= -\tilde{n}(-1) + M_{e-}\tilde{n}(-1)\exp(-(\Psi(-1) - \Psi_A))$$

i.e.,

$$\Psi_A - \Psi(-1) = \ln\left[\frac{1 + \tilde{I}/n(-1)}{M_{e-}}\right], \tag{18}$$

where $\tilde{\Gamma}_e$ is the normalized electron flux, A and C represent the anode and cathode near $x=-1$ and $x=1$, respectively, and

$$\tilde{n}M_{e\pm} = \frac{1}{c_s}\int_{v \gtrless 0} f_{\max}(\tilde{n}, T_e) v\, dv$$

is the normalized one-sided electron thermal flux. Using Eqs. (17) and (18), Eq. (16) becomes

$$\Delta\Psi = -[\Psi(1) - \Psi(-1)] + \ln\left[\frac{1 + \dfrac{\tilde{I}}{n(-1)}}{1 - \dfrac{\tilde{I}}{n(+1)}}\right] \tag{19}$$

Integrating Eq. (4) from -1 to 1 yields an expression for $\Psi(+1) - \Psi(-1)$:

$$\Psi(+1) - \Psi(-1) = \ln\left(\frac{\tilde{n}(1)}{\tilde{n}(-1)}\right) + \int_{-1}^{1} \frac{m_e \nu_e v_e L}{T_e} d\xi'. \tag{20}$$

Appendix A, Eq. (A7) yields

$$\frac{m_e \nu_e v_e L}{T_e} = \frac{c_s^2}{\bar{v}_e^2}\frac{4}{\sqrt{2}\pi}\frac{L}{\lambda_{\text{mfp}}}\frac{\bar{v}_e}{c_s}\frac{v_e}{c_s} = \frac{v_e}{\bar{v}_e}\frac{\alpha}{\tilde{M}}. \tag{21}$$

For a one-dimensional (1-D) system $\frac{1}{2}m\bar{v}_e^2 = \frac{1}{2}T_e$. Equations (3), (19), (20), and (21) then yield

$$\Delta\Psi = \ln\left[\frac{\tilde{n}(-1) + \tilde{I}}{\tilde{n}(+1) - \tilde{I}}\right] - \frac{\alpha\mu}{\tilde{M}}\sqrt{1 + \frac{\gamma}{\tau}}\int_{-1}^{1}\left(M - \frac{\tilde{I}}{\tilde{n}}\right) d\xi', \tag{22}$$

which yields the $I-V$ characteristics for the model system.

III. SOLUTION PROCEDURE

The solution process would normally involve the following steps.

(1) Determination of α and δ from the system parameters.
(2) Guess ξ_0 and integrate ξ from the boundaries. By the nature of the equation, $\xi \to \xi_0$ as $M \to 0^{\pm}$, but the slopes at $\xi_0^{\pm}$ may not match.
(3) Iterate until the correct ξ_0 is obtained.

While this scheme would work, integration up to a singularity is numerically noisy and the value of $\lim_{\xi\to\xi_0} d\xi/dM$ is not reliably obtainable.

An alternate scheme is therefore used that avoids these problems.

(1) Equation (12) is replaced by an auxiliary equation,

$$\frac{d\eta}{d\tilde{M}} = \frac{(1-\tilde{M}^2)}{\tilde{M}}\frac{\eta}{\tilde{\alpha}\tilde{M}\eta\left[\sqrt{1 + \frac{\pi}{8}\frac{\tilde{M}^2}{\bar{M}^2}} + \mu\sqrt{\tau}\right] + (1 + \tilde{M}^2 - 2\delta\tilde{M})}, \quad 0 \leqslant \tilde{M} \leqslant 1, \tag{23}$$

with $\eta \to 0^+$ as $\tilde{M} \to 0$ and

$$\lim_{\tilde{M}\to 0^+}\frac{d\eta}{d\tilde{M}} = 1.$$

(2) The singularity at $\tilde{M}=0$ is resolved by using an analytic approximation for $\tilde{M}(\eta)$ derived in Appendix C that is accurate to $\mathcal{O}(\eta^3)$:

$$\tilde{M} = \eta\left[1 - 2\tilde{\delta}\eta + \frac{\eta^2}{2}(\tilde{\alpha}(1 + \mu\sqrt{\tau}) + 2 + 8\tilde{\delta}^3)\right] + \mathcal{O}(\eta^4). \tag{24}$$

For prescribed tolerance ϵ, Eq. (24) is used in the region $-\eta_{\text{cr}} < \eta < \eta_{\text{cr}}$, where

$$\eta_{\text{cr}} = \left(\frac{2\epsilon}{\tilde{\alpha}(1 + \mu\sqrt{\tau}) + 2 + 8\tilde{\delta}^2}\right)^{1/3} \tag{25}$$

(3) Equation (23) is now solved in the regions $\eta < -\eta_{\text{cr}}$ and $\eta > \eta_{\text{cr}}$, thus yielding a complete solution.

(4) Steps (2) and (3) are carried out for some $\tilde{\alpha}_+$ and $\tilde{\delta}$ to yield

$$\eta_+(\tilde{M}) = \eta(\tilde{M}; \tilde{\alpha}_+, \tilde{\delta}), \quad 0 < \tilde{M} \leqslant 1. \tag{26}$$

Steps (2) and (3) are also carried out for some $\tilde{\alpha}_-$ but with $-\tilde{\delta}$:

$$\eta_-(\tilde{M}) = \eta(\tilde{M}; \tilde{\alpha}_-, \tilde{\delta}), \quad 0 < \tilde{M} \leqslant 1. \tag{27}$$

(5) Solutions (26) and (27) are now used to construct a valid solution of (11). Equation (26) is mapped into $\xi \in (\xi_0, 1]$ by the transformation

$$\xi = \xi_0 + (1 - \xi_0)\frac{\eta_+(M)}{\eta_+(1)}, \quad 0 < \tilde{M} \leqslant 1 \tag{28}$$

and Eq. (27) is mapped into $\xi \in [-1, \xi_0)$ by the transformation

$$\xi=\xi_0-(1+\xi_0)\frac{\eta_-(-M)}{\eta_-(1)},\quad -1\leqslant\tilde{M}<0. \tag{29}$$

Both Eqs. (28) and (29) transform Eq. (23) into Eq. (12) and ensure that the boundary conditions at $M=\pm 1$ are satisfied. However, the solution should also be continuous (automatically true) and have a continuous derivative at $\xi=\xi_0$. [The need for a continuous derivative results from Eq. (10), since $n(\xi)$ must clearly be continuous at $\xi=\xi_0$.] In addition, both Eqs. (28) and (29) should correspond to the same set of system parameters, α and δ. These considerations yield the following two conditions:

$$\frac{1-\xi_0}{\eta_+(1)}=\frac{1+\xi_0}{\eta_-(1)} \tag{30}$$

and

$$\tilde{\alpha}_+(\xi-\xi_0)\frac{\eta_+(1)}{1-\xi_0}=\tilde{\alpha}_-(\xi-\xi_0)\frac{\eta_-(1)}{1+\xi_0}=\alpha(\xi-\xi_0). \tag{31}$$

Equation (30) immediately yields the value of ξ_0:

$$\xi_0=\frac{\eta_-(1)-\eta_+(1)}{\eta_-(1)+\eta_+(1)}, \tag{32}$$

while Eq. (31) implies

$$\tilde{\alpha}_+=\tilde{\alpha}_-=\tilde{\alpha}=\alpha\frac{1-\xi_0}{\eta_+(1)}. \tag{33}$$

Using Eq. (32) this becomes

$$\tilde{\alpha}=\alpha\frac{2}{\eta_-(1)+\eta_+(1)}. \tag{34}$$

Since $\eta_+(1)$ and $\eta_-(1)$ are determined as part of the solution process, Eq. (34) cannot be used to predetermine the value of $\tilde{\alpha}$ that will yield the desired value of α. Thus iteration is still required to obtain the solution corresponding to a specific choice of machine parameters. However, this approach has the following two significant advantages (besides avoiding the problem of integrating the equations toward a singularity).

(1) Parametric studies require no iteration. However, the points in (α,δ) space are not on a grid, complicating interpolation studies.

(2) Even if the iteration to achieve some α_0 has a residual error, that error is more tolerable, since there is a value of α near α_0 for which the solution is exact. *Hence, unphysical properties will not appear in the solution.*

IV. ANALYTICAL MODEL

The collision frequency obtained in Appendix A assumes that ions scatter of a thermal distribution of equally massive neutrals. This results in an operator that approaches constant collision frequency at low velocities, and approaches constant mean free path at high velocities. In this section this operator is approximated by a constant collision frequency operator at all velocities. Then Eq. (23) simplifies to

$$\frac{dM}{d\xi}-\frac{\alpha M^2(1+\mu\sqrt{\tau})}{(1-M^2)}=\frac{M}{\xi-\xi_0}\left[\frac{1+M^2-2\delta M}{1-M^2}\right]. \tag{35}$$

This can be written as

$$\frac{1-M^2}{M(1+M^2)}\frac{dM}{d\xi}-\frac{1}{\xi-\xi_0}=\bar{\alpha}\frac{M}{1+M^2}-\frac{2\delta}{(\xi-\xi_0)}\frac{M}{(1+M^2)}, \tag{36}$$

where $\bar{\alpha}=\alpha(1+\mu\sqrt{\tau})$. The left-hand side of Eq. (36) is a perfect derivative:

$$\frac{d}{d\xi}\left[\ln\left(\frac{M}{1+M^2}\right)\right]-\frac{d}{d\xi}(\ln(\xi-\xi_0))=\bar{\alpha}\frac{M}{1+M^2}-\frac{2\delta}{(\xi-\xi_0)}\frac{M}{(1+M^2)}. \tag{37}$$

Equation (36) can be reduced to a linear equation by the transformation $w=(1+M^2)/M$, which yields

$$\frac{d}{d\xi}(w(\xi-\xi_0))=-\bar{\alpha}(\xi-\xi_0)+2\delta \tag{38}$$

with a solution

$$w=-\frac{\bar{\alpha}}{2}(\xi-\xi_0)+2\delta+\frac{C}{\xi-\xi_0}, \tag{39}$$

where C and ξ_0 are constants yet to be determined. The requirement that $w=\pm 2$ at $\xi=\pm 1$ yields the following values of C and ξ_0:

$$\begin{aligned} C&=2(1-\xi_0)(1-\delta)+\frac{\bar{\alpha}}{2}(1-\xi_0)^2,\\ \xi_0&=-\frac{2\delta}{2+\alpha(1+\mu\sqrt{\tau})}. \end{aligned} \tag{40}$$

Equation (39) can be expressed as a quadratic equation for M,

$$M^2-bM+1=0, \tag{41}$$

where

$$b=-\frac{\bar{\alpha}}{2}(\xi-\xi_0)+2\delta+\frac{C}{(\xi-\xi_0)}. \tag{42}$$

The solutions yield expressions for M and $n=(\xi-\xi_0)/M$,

$$M=\frac{b-\sqrt{b^2-4}}{2},\quad n=\frac{\xi-\xi_0}{\frac{b}{2}-\sqrt{\frac{b^2}{4}-1}}. \tag{43}$$

Equation (43) is an exact, nonlinearly correct solution for the system when collisions may be modeled by a constant collision frequency. Such a model is excellent for bulk plasma but invalid near the walls, where $M\gg\bar{M}$. While invalid near $\xi=\pm 1$, Eq. (43) retains the square-root singularity near the

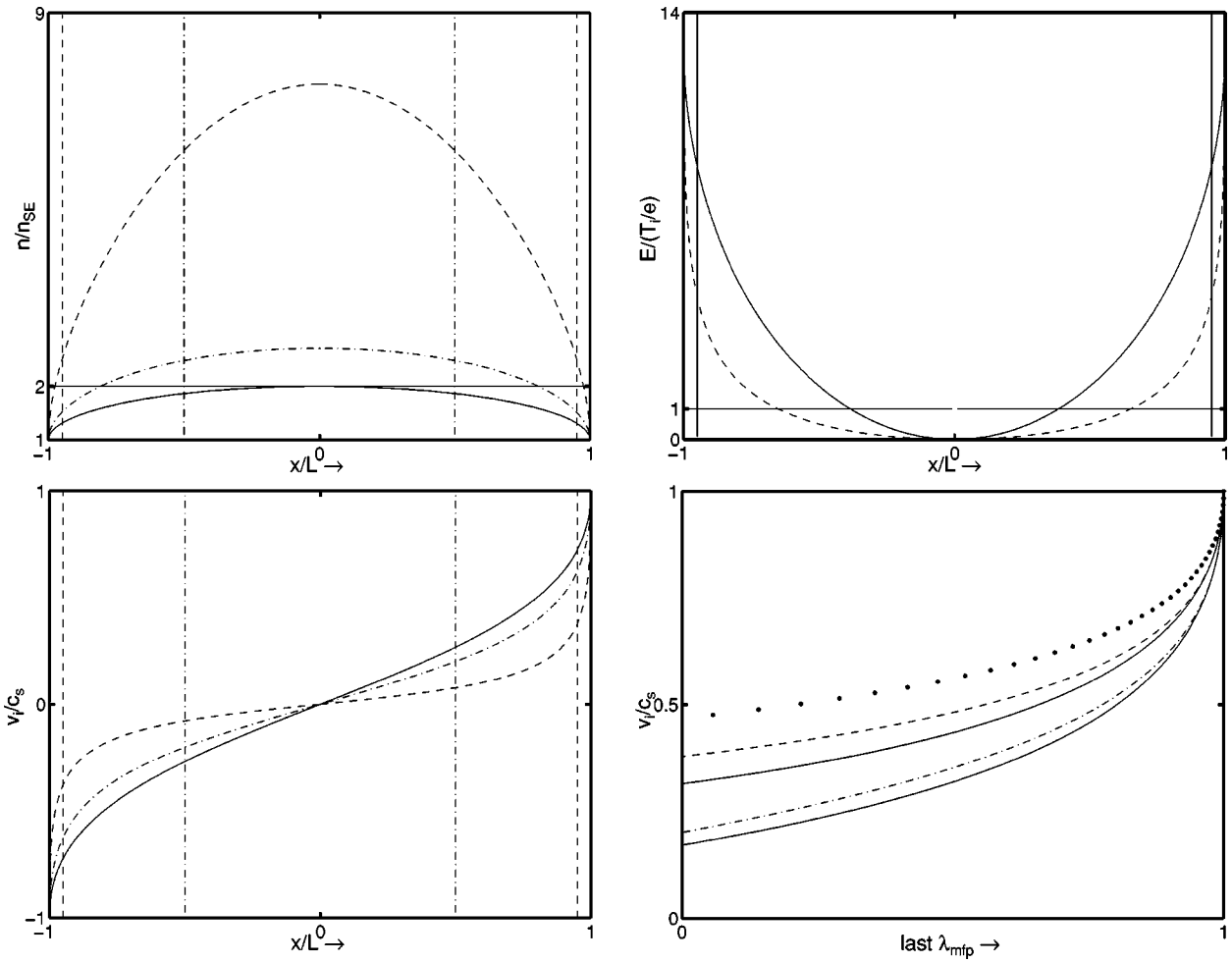

FIG. 2. Profiles generated for zero current by the solution of (11). In (a)–(c), the solid curves represent the collisionless ($\nu=0$) case, the dot-dash curves represent a case where $\lambda_{mfp}=L/2$, and the dashed curves represent a case where $\lambda_{mfp}=L/20$. In all cases, $T_i=0.1T_e$ has been assumed. Vertical lines indicating the beginning of the last λ_{mfp} have been drawn in the respective line style. (a) Density profiles scaled to edge density. The curves demonstrate the smooth connection between a collisional, ambipolar bulk plasma with the presheath region. (b) Velocity profiles scaled to $c_s=(T_e+\gamma T_i)/m_i$. The profiles are nearly linear in the bulk region where the plasma is ambipolar. The slopes of the profiles at $\xi=0$ are inversely proportional to the central density. (c) For $\nu=0$ and $\lambda_{mfp}=L/20$, the ion kinetic energy scaled to ion temperature is plotted. As the system becomes increasingly collisional, the drift energy does drop compared to the $\nu=0$ case, but it is interesting to observe that ions have super-thermal drifts well away from the last mean free path. For the case of $\lambda_{mfp}=L/20$, ion drifts reach v_i eight λ_{mfp} from the wall. (d) The ion velocity scaled to c_s plotted against $(L-x)/\lambda_{mfp}$. The dashed and dot-dashed lines use the same λ_{mfp} as the previous plots. The top and bottom solid lines indicate values of M obtained from Eq. (43) with $\lambda_{mfp}=L/20$ and $\lambda_{mfp}=L/2$, respectively. The dotted line indicates the infinite collisionality case from (45). The entry velocities are seen to increase with collisionality.

wall. Since both M and n are known analytically, the potential drop given in Eq. (22) can also be obtained, to yield $I-V$ characteristics.

V. RESULT AND DISCUSSION

The numerical algorithm described in Sec. III was implemented in a FORTRAN 77 program. The nature of the solutions obtained are described in the following paragraphs. Where relevant, limits from ambipolar theory and from Sec. IV are presented.

The density profile scaled to n_{SE}, the edge density, is presented in Fig. 2(a) for three different collision frequencies. The solid curve corresponds to zero collision frequency and agrees with the standard presheath result. For this case, the presheath is the size of the system, and $n_{bulk}/n_{SE}=2$. The dot-dash curve corresponds to a weakly collisional plasma, with $\lambda_{mfp}/L=0.5$. For this case, the vertical lines at $\xi=\pm 0.5$ represent the start of the ''last mean free path'' near the wall. As is seen in Fig. 2(a), the density rises to higher than twice n_{SE} in this region. Of course, it rises further in the interior of the plasma, but that corresponds to the bulk region which should be dominated by ambipolar diffusive processes. The dashed curve in Fig. 2(a) is a highly collisional case, with $\lambda_{mfp}/L=0.05$. The relevant vertical lines now are those at $\xi=\pm 0.95$. Once again, the density rises to above the conventional value of $2n_{SE}$.

This excess of density can be interpreted in the following manner. The last mean free path from the wall is a region where ions gain kinetic energy from the field. Quasineutrality links the field and the pressure through the electrons, which are nearly Boltzmann. Thus, in the fluid equations, the momentum source for ions is the pressure gradient. When collisions are present, they absorb some of the momentum

gained, and so additional momentum needs to be supplied by the pressure profile. This results in a steepened density profile, and therefore an increased value for the bulk density relative to the sheath density.

The velocity profiles for the above-mentioned three cases are presented in Fig. 2(b). As collisions increase, the simple collisionless presheath expression,

$$\xi = M/(1+M^2),$$

is replaced by a boundary layer type of profile. The slope at $\xi=0$ is inversely proportional to the central density, and the linearity of the profile in the bulk is the extent to which the density is uniform.

The kinetic energy of ions is presented in Fig. 2(c), scaled to the ion thermal energy. The purpose of this plot is to investigate the true size of the presheath region. The presheath may always be *defined* as the last λ_{mfp}, but the validity of this definition depends on whether the rest of the plasma can be accurately represented by equations that assume weak flows. If the criterion for ''weakness'' is $u_i < v_i$, i.e., the fluid flow velocity is less than the ion thermal velocity, Fig. 2(c) shows that the criterion yields a far larger region than expected. For the $\lambda_{\mathrm{mfp}}/L=0.05$ case the flow is super-thermal up to $8\lambda_{\mathrm{mfp}}$ from the wall.

Flows could also be defined as ''weak'' if they are much smaller than c_s. Figure 2(d) presents the velocity profiles of the above-mentioned cases superposed over their respective last λ_{mfp}. It is now clear that the inlet velocity into the last λ_{mfp} region increases with collisionality. The solid lines in Fig. 2(d) are the curves generated by Eq. (43) for the corresponding system parameters. As has been noted in Sec. IV, Eq. (43) assumes a constant collision frequency. To make a useful comparison to numerical output, the collision frequency used was that at the wall, i.e., α was increased by a factor $(\sqrt{1+(1/\bar{M}^2)(\pi/8)}+\mu\sqrt{\tau})/(1+\mu\sqrt{\tau})$ over its bulk value. Recognizing the inflated $\alpha(1+\mu\sqrt{\tau})$ as L/λ_{mfp} itself, Eq. (43) becomes with $\delta=0$,

$$M = \frac{L/\lambda_{\mathrm{mfp}}}{4}(\xi^{-1}-\xi)+\frac{1}{\xi} - \sqrt{\left(\frac{L/\lambda_{\mathrm{mfp}}}{4}(\xi^{-1}-\xi)+\frac{1}{\xi}\right)^2-1}. \tag{44}$$

Defining $\zeta = L/\lambda_{\mathrm{mfp}}(1-\xi)$, Eq. (44) may be rewritten

$$M = \frac{\zeta}{2}\frac{(1+\xi)}{2\xi}+\frac{1}{\xi}-\sqrt{\frac{\zeta^2}{4}\left(\frac{(1+\xi)}{2\xi}\right)^2-1}. \tag{45}$$

The $\alpha\to\infty$ solution is obtained by setting $\xi=1$ in Eq. (45). This is the dotted line shown in Fig. 2(d). Equation (45) yields an asymptotic value for the inlet velocity [i.e., $M(\zeta=1)$] of 0.382. The numerical value is higher since the collision frequency drops even in this region, an effect that is absent in Eq. (45). Nonetheless, the numbers indicate that most of the kinetic energy is gained in the last λ_{mfp}, even though the ion flow energy dominates the temperatures well inside the bulk.

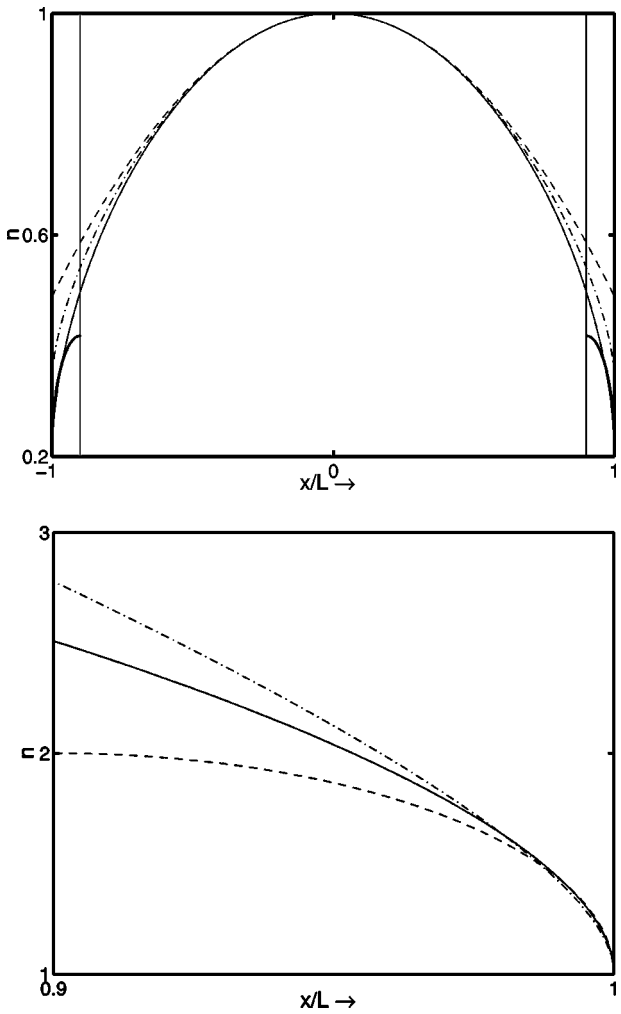

FIG. 3. (a) The density profile is displayed for the case of $I_p=0$, $\lambda_{\mathrm{mfp}}=0.1L$, $T_e/T_i=10$, and $m_i=m_p$. The solid line is the simulation result. The dashed line refers to the density from ambipolar theory. The dot-dashed line represents the expression given in Eq. (43). The vertical lines show the start of the last mean free path of the system. The thick solid lines between the walls and the last λ_{mfp} show the standard presheath prediction. For both the ambipolar curve and for Eq. (43), the plotted curves have been shifted vertically to make their peaks coincide with the numerical results, as they are most valid in the bulk plasma. (b) The density profile over the last λ_{mfp} is displayed for the case of $I_p=0$, $\lambda_{\mathrm{mfp}}=0.1L$, $T_e/T_i=10$, and $m_i=m_p$. The solid curve is the simulation result and the dashed curve is the ideal presheath result. The dot-dashed line is the curve from Eq. (43). The dotted line represents the curve obtained from Eq. (43), when the collision frequency is enhanced to match the correct value at the wall.

Figure 3(a) presents the density profile for the case of $L=10\lambda_{\mathrm{mfp}}$, $T_e=10T_i$, $m_i=m_p$, and $I_p=0$. The solid line is the numerical solution. The ideal presheath profiles (solid lines) are shown for reference. The dashed line is the ambipolar result and the dot-dashed curve is obtained from Eq. (43). Both these curves have been vertically shifted to coincide with the numerical curve at $\xi=0$, since they are most valid in the bulk. It can be seen that the numerics deviates from both theoretical curves well away from the wall. This is due to the velocity dependence of the collision operator.

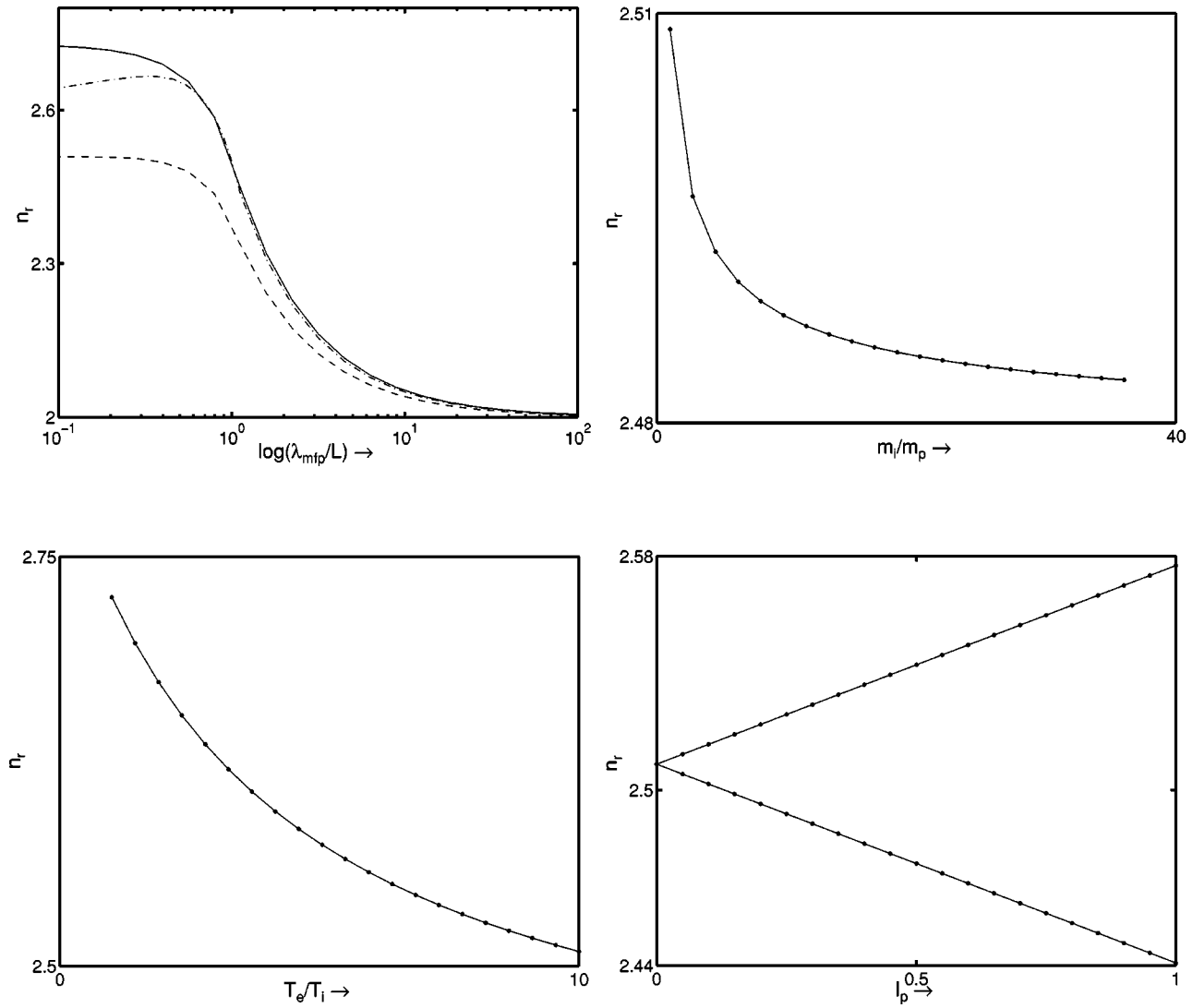

FIG. 4. Ratio (n_r) of density at the last λ_{mfp} to the density at the wall as a function of different parameters: (a) $m_i/m_p=1$, $I_p=0$ $T_e/T_i=10$ for the dashed, curve and $T_e/T_i=1.0$ for the solid line for different λ_{mfp}. The dot-dashed line is for analytical result obtained from Eq. (46) for $T_e/T_i=1.0$. (b) $m_i/m_p=1$, $\lambda_{mfp}=0.1L$, $I_p=0$ and varying T_e/T_i. (c) $T_e/T_i=10$, $\lambda_{mfp}=0.1L$, $I_p=0$ and varying m_i/m_p. (d) $m_i/m_p=1$, $\lambda_{mfp}=0.1L$, $T_e/T_i=10$ and varying I_p. The rising curve represents n_r at the anode ($\xi=-1$), while the falling curve represents n_r at the cathode side ($\xi=1$).

Closer to the wall, the theoretical result deviates from the ambipolar result as it must develop the square root singularity at $\xi=\pm 1$. It is worth noting here that the ambipolar result plotted here uses $\gamma=1$ consistent with the assumption of that theory, while the other curves use $\gamma=3$. Nonetheless, excellent agreement is obtained in the bulk, which suggests that the deficiency in Eq. (8) is not serious.

It is worth noting here that a fully ionized plasma would scatter according to the Coulomb collision operator. For ambipolar flow, the relevant collision frequency is $\nu_s^{i/e}$, which is independent of ion velocity for $v_i \ll \bar{v}_e$.[18] Since this inequality prevails here, the theoretical result in Eq. (43) should be reasonably accurate for fully ionized plasma columns. Of course, the use of the Krook operator[19] to model collisions in such a plasma is very questionable.

Figure 3(b) displays the density profile over the last λ_{mfp} for the same case as in Fig. 3(a). The solid curve is the numerical result, while the dashed curve is the ideal presheath result. The dot-dashed curve is the result of Eq. (43), with α enhanced by the factor $(\sqrt{1+(\pi/8\bar{M}^2)}+\mu\sqrt{\tau})/(1+\mu\sqrt{\tau})$ to account for the higher collision frequency near the wall. This value is actually too high except at $\xi=1$ itself, and hence the predicted density is higher than the numerical value.

Figure 4 presents parametric studies of n_r, the ratio of ''bulk density'' (defined to be the density one λ_{mfp} from the wall) to ''edge density'' [i.e., $n(\xi=\pm 1)$]. Figure 4(a) presents the variation of n_r with λ_{mfp}. When $\lambda_{mfp}>L$, n_r is alternatively defined to be the ratio of central density to edge density. In Figs. 4(b), 4(c), and 4(d) $\lambda_{mfp}<L$ holds for all curves, but in Fig. 4(a), λ_{mfp} ranges from $0.1L$ to $100L$. The solid line in Fig. 4(a) corresponds to $T_e=T_i$ while the dashed line corresponds to $T_e=10T_i$. As is seen, a higher ratio of densities is achieved for $\lambda_{mfp} \ll L$ when $T_e \sim T_i$, but the curves agree when $\lambda_{mfp} \gg L$. These results may be under-

stood by setting $\xi=1-\lambda_{mfp}/L$ and $\zeta=1$ in Eq. (45):

$$M_{PS}=\frac{6L/\lambda_{mfp}-1}{4L/\lambda_{mfp}-4}-\sqrt{\left(\frac{6L/\lambda_{mfp}-1}{4L/\lambda_{mfp}-4}\right)^2-1},$$

$$L\neq\lambda_{mfp}. \tag{46}$$

For $\lambda_{mfp}<L$, Eq. (46) yields $n_r=(1-\lambda_{mfp}/L)/M_{PS}$ while for $\lambda_{mfp}>L$, Eq. (43) yields $n_r=2+L/(2\lambda_{mfp})$. These expressions are plotted in Fig. 4(a) as the dot-dashed curve. Since Eq. (46) is a constant collision frequency curve, it cannot expect to recover numerical results. However, it should agree best with that case whose collision frequency varied least, namely the $T_e=T_i$ curve. As $\lambda_{mfp}\to 0$, particle conservation in the presheath becomes increasingly valid: $n_{PS}M_{PS}=1$. The drop in n_r for the theoretical curve is due to the nonsaturation of M_{PS} as $\lambda_{mfp}\to 0$. The numerical curves show a saturation which the authors believe is due to most of the n_r value coming from the very edge before the effective collision frequency starts to drop.

Figure 4(b) explores the dependence of n_r on T_e/T_i. The dominant effect is on $\bar{M}$ which drops with increasing T_e/T_i. The effective collision frequency is given by

$$\alpha\left(\sqrt{1+\frac{\pi M^2}{8\bar{M}^2}}+\mu\sqrt{\tau}\right)\approx\frac{L}{\lambda_{mfp}}\sqrt{M^2+\frac{8\bar{M}^2}{\pi}}. \tag{47}$$

At the wall the effective collision frequency is nearly independent of $\bar{M}$. Away from the wall, it decreases with decreasing $\bar{M}$, i.e., with increasing T_e/T_i. Following the argument given in connection with Fig. 2(a), increasing T_e/T_i results in a decrease in n_r. As Fig. 4(b) demonstrates, the effect is significant, as $n_r=2.7$ at $T_e=T_i$ and $n_r\to 2.5$ as $T_e/T_i=10$. It should be noted that this effect is missing in Eq. (44), which yields a value of n_r that is independent of T_e/T_i.

Figure 4(c) presents the variation of n_r as a function of m_i/m_p. The only place where m_i/m_p enters in Eq. (12) at zero current is through the electron drag term, $\mu\sqrt{\tau}$. Increasing m_i/m_p reduces $\mu=\sqrt{m_e/m_i}$, thereby reducing the collisional term. This explains the marginal reduction in n_r. The overall importance of this term given approximately by $\mu\sqrt{\tau}/(1+(\pi/8)(1/\bar{M}^2))\sim 0.012\sqrt{(m_i/m_p)}$, which explains the order of variation in n_r.

Figure 4(d) displays the effect of an external current on n_r, the falling curve represents the cathode presheath near $\xi=1$, while the rising curve represents the anode presheath near $\xi=-1$.

Figure 5 shows the $I-V$ characteristics of the model system. The solid line is the result of using the numerical solution in Eq. (22). The dotted line shows the ambipolar result and the dashed line is the result of using Eq. (43) in Eq. (22). There is an excellent agreement between the constant ν theory and the numerical result, both of which deviate from the ambipolar result at higher current. This deviation may be understood as follows: When current flows through the system, the location, ξ_0, where $M=0$ shifts according to Eq. (40). For positive current ($\delta>0$), the shift is negative. All the ions injected by the source in the region $\xi_0<\xi<1$ must necessarily flow to the wall at $\xi=1$, i.e., to the cathode. Since the inlet velocity to the sheath is always c_s, the increased flux of particles is reflected in an increase in the sheath-edge density $n(1)$. Thus, the ion saturation current exceeds its ambipolar value by a factor $1-\xi_0=1+2\delta/(2+\bar{\alpha})$. This is a 6% effect for the parameters used in Fig. 5. If an emissive wall were used, δ could be much larger, and this effect enhanced.

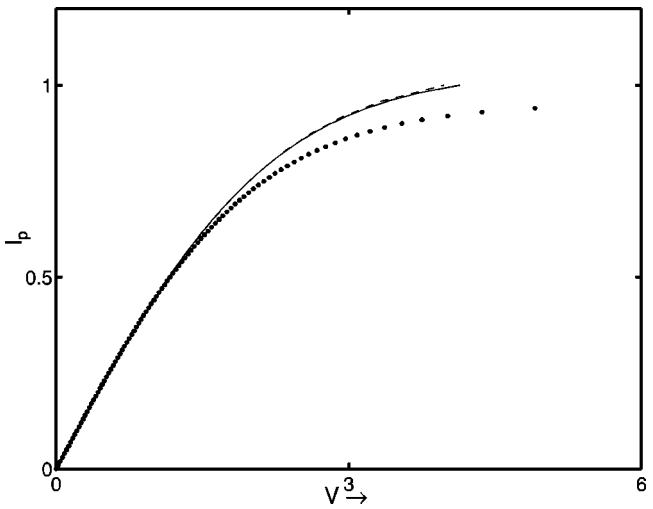

FIG. 5. $I-V$ characteristics for the system. The solid line is the simulation result. The dashed line is the result of using Eq. (43) in Eq. (22). The dotted line is the result of using Eqs. (B5) and (B7) in Eq. (22), and represents the ambipolar prediction. For all these curves $\alpha=4.0$ has been used.

To summarize, this paper presents a formulation of a 1-D plasma column that self-consistently includes both bulk and presheath physics. An analytic solution was derived for the interesting limit where the collision operator is independent of flow velocities. Significant findings include a shift in the bulk to sheath density ratio for even moderately collisional systems, a change in the $I-V$ characteristics, and super-thermal ion flow in the bulk plasma.

ACKNOWLEDGMENTS

The authors gratefully acknowledge the critical comments by R. Ganesh, especially on the choice of collision frequency. M.G. thanks D. Sharma for helpful discussions on numerical methods.

APPENDIX A: MODEL FOR COLLISIONS

For a system dominated by collisions with neutrals, the collision frequency may be obtained from simplistic kinetic theory. Assuming a Krook collision operator, the collisional flux of velocity is given by

$$-\nu_i n_i v_i\equiv\int_{-\infty}^{\infty}(-n_0\sigma|v|)(f_i(v)-f_0(v))v\,dv, \tag{A1}$$

where $f_i(v)=n_i\sqrt{m_i/2\pi T_i}\,\exp(-m_i(v-v_i)^2/2T_i)$ is the distribution function for the ions, assumed (consistent with the use of fluid theory) to be a drifting Maxwellian, $f_0(v)=n_{00}\sqrt{m_i/2\pi T_i}\,\exp(-m_i v^2/2T_i)$ the distribution to which the ions are collisionally relaxing, and $n_0\sigma|v|$ the collision frequency. The neutrals are assumed to be at the same temperature as the ions, and n_{00} chosen to make Eq. (A1) particle conserving.

Assuming that the collision cross-section for ion–neutral collisions is velocity independent, Eq. (A1) becomes for f_i and f_0:

$$-\nu_i n_i v_i=-n_0\sigma\left(n_i\sqrt{\frac{m_i}{2\pi T_i}}\right)\int_{-\infty}^{\infty}v|v|e^{m_i(v-v_i)^2/2T_i}\,dv, \tag{A2}$$

where the term involving f_0 drops out due to antisymmetry. Transforming to $\chi^2=m_i v^2/T_i$ ($\chi d\chi=m_i v\,dkv/T_i$), Eq. (A2) becomes

$$-\nu_i n_i v_i=-\frac{n_0 n_i\sigma}{\sqrt{2\pi}}\frac{T_i}{m_i}\int_0^{\infty}\chi^2(e^{-(\chi-\chi_i)^2/2}-e^{-(\chi+\chi_i)^2/2})d\chi. \tag{A3}$$

The integral is expressible in the form of error functions:

$$-\nu_i n_i v_i=-\frac{n_0 n_i\sigma}{\sqrt{2\pi}}\frac{T_i}{m_i}\left[\sqrt{2\pi}(\chi_i^2+1)\,\mathrm{erf}\left(\frac{\chi_i}{\sqrt{2}}\right)+2\chi_i\exp\left(\frac{-\chi_i^2}{2}\right)\right], \tag{A4}$$

where $\chi_i=v_i\sqrt{m_i/T_i}$ is the normalized fluid velocity.

A simple fit to (A4) that is correct to within 2% relative error over $0<\chi<5$ is given by

$$\left[\sqrt{2\pi}(\chi_i^2+1)\,\mathrm{erf}\left(\frac{\chi_i}{\sqrt{2}}\right)+2\chi_i\exp\left(\frac{-\chi_i^2}{2}\right)\right]=4\chi_i\sqrt{1+\frac{\pi}{8}\chi_i^2}. \tag{A5}$$

This approximation may be understood as saying that at low fluid velocities, the ion collision frequency is determined primarily by the thermal velocity; at higher fluid velocities, the collision frequency is determined primarily by the fluid velocity. The above-mentioned approximation yields a simple expression for the collision term:

$$(-\nu_i n_i v_i)\frac{L}{n_i c_s^2}=-\left(\frac{4}{\sqrt{2\pi}}\frac{L}{\lambda_{\mathrm{mfp}}}\bar{M}\right)M\sqrt{1+\frac{\pi}{8}\frac{M^2}{\bar{M}^2}}. \tag{A6}$$

Defining $\alpha=4L\bar{M}/\sqrt{2\pi}\lambda_{\mathrm{mfp}}$, this yields the expression used in (8).

For electrons, the same analysis with the additional simplification that $v_e\ll\bar{v}_e$ yields

$$\frac{L\nu_e}{c_s}=\alpha\sqrt{\frac{m_i}{m_e}\frac{T_e}{T_i}}, \tag{A7}$$

where $M_e=\bar{v}_e/c_s$.

The validity of this analysis for electrons requires discussion, since electrons cannot thermalize through such collisions (due to the large mass ratio). Thus this result is to be understood as the rate at which the directed velocity of the electrons decays through isotropization.[20] Further thermalization occurs by scattering off other electrons via Coulomb interactions. It should be noted that while electron–neutral collisions can only isotropize the electron distribution, the electron–electron collisions (ν_{ee}) can only thermalize the electrons. ν_{ee} collisions cannot reduce the fluid drift velocity of electrons and hence the appropriate frictional drag term for the electron fluid is Eq. (A7).

APPENDIX B: EQUATIONS FOR AN EQUIVALENT AMBIPOLAR SYSTEM

In this treatment the plasma is modeled as an ambipolar fluid. Electrons and ions diffuse due to collisions. Because of the ambipolar electric field created due to the charge separation between the electrons and ions, electron flow is retarded and ion flow is accelerated. The dynamics are governed by the steady state ambipolar diffusion equation.

$$-D_a\frac{d^2n}{dx^2}=S. \tag{B1}$$

The ion and electron fluxes are given by

$$\Gamma_i=\mu_i nE-D_i\frac{dn}{dx},\quad \Gamma_e=-\mu_e nE-D_e\frac{dn}{dx}, \tag{B2}$$

where D_a is the ambipolar diffusion coefficient given by $D_a=(\mu_e D_i+\mu_i D_e)/(\mu_e+\mu_i)$, $\mu_s=|q|/m_s\nu_s$ is the mobility of species s, and $D_s=T_s/m_s\nu_s$ is its diffusion coefficient.[12] In terms of the notation followed in this paper, D_a may be written as

$$\tilde{D}_a=\frac{D_a}{Lc_s}=\frac{1}{\alpha(1+\mu\sqrt{\tau})}, \tag{B3}$$

and Eq. (B1) becomes

$$-\tilde{D}_a\frac{d^2\tilde{n}}{d\xi^2}=\frac{LS}{n_0c_s}=1, \tag{B4}$$

which yields

$$\tilde{n}(\xi)=-\frac{1}{2\tilde{D}_a}\xi^2+b\xi+c, \tag{B5}$$

where b and c are constants to be determined from the boundary conditions. The electric field, E, may be eliminated by combining Γ_i and Γ_e of Eq. (B2) to yield

$$\frac{\Gamma_i}{n_0c_s}=-\tilde{D}_a\frac{d\tilde{n}}{d\xi}+\frac{\mu_i}{\mu_e+\mu_i}\tilde{I}. \tag{B6}$$

At the sheath edge, the Bohm condition[21] gives

$$\frac{\Gamma_i(\pm1)}{n_0c_s}=\pm\tilde{n}_{\mathrm{edge}}=-\tilde{D}_a\frac{\partial}{\partial\xi}(\tilde{n}(\pm1))+\frac{\mu_i}{\mu_e+\mu_i}\tilde{I}. \tag{B7}$$

Equations (B5) and (B7) yield

$$b=\left(\frac{1}{1+\frac{1}{\mu\sqrt{\tau}}}\right)\frac{\tilde{I}}{1+\tilde{D}_a},\quad c=S\left(1+\frac{1}{2\tilde{D}_a}\right). \tag{B8}$$

This expressions have been used to generate Figs. 3 and 5.

APPENDIX C: SMALL η EXPANSION FOR $\tilde{M}$

For small $\tilde{M}$, Eq. (23) can be expanded to get

$$\frac{d\tilde{M}}{d\eta}-\tilde{\alpha}\tilde{M}^2(1+\mu\sqrt{\tau})(1+\tilde{M}^2)$$

$$=\frac{\tilde{M}}{\eta}(1+\tilde{M}^2)(1+\tilde{M}^2-2\tilde{\delta}\tilde{M}) \tag{C1}$$

with $d\tilde{M}/d\eta|_0=1$. To zeroth order Eq. (C1) becomes

$$\frac{d\tilde{M}^{(0)}}{d\eta}=\frac{\tilde{M}^{(0)}}{\eta}$$

with

$$\left.\frac{d\tilde{M}^{(0)}}{d\eta}\right|_0=1, \tag{C2}$$

which yields $\tilde{M}^{(0)}=\eta$.

To first order Eq. (C1) becomes

$$\frac{d\tilde{M}^{(1)}}{d\eta}=\frac{\tilde{M}^{(0)}}{\eta}(-2\tilde{\delta}\tilde{M}^{(0)})+\frac{\tilde{M}^{(1)}}{\eta}.$$

Substituting for $\tilde{M}^{(0)}$ yields $\eta(d/d\eta)(\tilde{M}^{(1)}/\eta)=-2\tilde{\delta}\eta$, which is solved to yield $\tilde{M}^{(1)}=-2\tilde{\delta}\eta^2$.

To second order Eq. (C1) is

$$\frac{d\tilde{M}^{(2)}}{d\eta}-\tilde{\alpha}(1+\mu\sqrt{\tau})\tilde{M}^{(0)^2}$$

$$=\frac{\tilde{M}^{(0)}}{\eta}(2\tilde{M}^{(0)^2}-2\tilde{\delta}\tilde{M}^{(1)})$$

$$+\frac{\tilde{M}^{(1)}}{\eta}(-2\tilde{\delta}\tilde{M}^{(0)})+\frac{\tilde{M}^{(2)}}{\eta}.$$

Substituting for $\tilde{M}^{(0)}$ and $\tilde{M}^{(1)}$, yields

$$\eta\frac{d}{d\eta}\left(\frac{\tilde{M}^{(2)}}{\eta}\right)=(\tilde{\alpha}(1+\mu\sqrt{\tau})+2+8\tilde{\delta}^2)\eta^2.$$

The solution is $\tilde{M}^{(2)}=(\tilde{\alpha}(1+\mu\sqrt{\tau})+2+8\tilde{\delta}^2)\eta^3/2$.

Hence the total solution, i.e., $\tilde{M}^{(0)}+\tilde{M}^{(1)}+\tilde{M}^{(2)}$, accurate to $\mathcal{O}(\eta^3)$ is represented by Eq. (24),

$$M=\eta-2\tilde{\delta}\eta^2+(\tilde{\alpha}(1+\mu\sqrt{\tau})+2+8\tilde{\delta}^2)\frac{\eta^3}{2}+\mathcal{O}(\eta^4). \tag{C3}$$

Equation (24) is valid in the region $(0,\eta_{cr})$, where η_{cr} is the point at which analytical solution is unacceptable. The error is estimated as the $\mathcal{O}(\eta^3)$ term

$$(\tilde{\alpha}(1+\mu\sqrt{\tau})+2+8\tilde{\delta}^2)\frac{\eta^3}{2}\leqslant\epsilon, \tag{C4}$$

which yields the criterion Eq. (25).

[1] L. Tonks and I. Langmuir, Phys. Rev. **34**, 876 (1929); **33**, 1070 (1929).
[2] I. Langmuir, Phys. Rev. **33**, 954 (1929).
[3] L. D. Thornhill, J. Plasma Phys. **59**, 505 (1998).
[4] K.-U. Riemann, J. Phys. D: Appl. Phys. **24**, 493 (1991), and references thereafter.
[5] K.-U. Riemann and P. Meyer, Phys. Plasmas **3**, 4751 (1996).
[6] H.-B. Valentini, Phys. Plasmas **3**, 4754 (1996).
[7] F. F. Chen, J. Nucl. Energy, Part C **7**, 47 (1965).
[8] J. B. Blank, Phys. Fluids **11**, 1686 (1968).
[9] H.-B. Valentini, E. Glauche, and D. Wolff, Plasma Sources Sci. Technol. **4**, 353 (1995).
[10] I. G. Kouzentsov, A. J. Lichtenberg, and M. A. Lieberman, Plasma Sources Sci. Technol. **5**, 662 (1996).
[11] Y. Lin and R. A. Adomaitis, Phys. Lett. A **243**, 142 (1998).
[12] F. F. Chen, *Plasma Physics,* Plasma Physics and Controlled Fusion Vol. 1 (Plenum, New York, 1984), Chap. 5, p. 55.
[13] R. N. Franklin, *Plasma Phenomena in Gas Discharges* (Clarendon, Oxford, 1976), Chap. 4, p. 51.
[14] J. T. Scheuer and G. A. Emmert, Phys. Fluids B **2**, 445 (1990).
[15] R. Chodura, Phys. Fluids **25**, 1628 (1982).
[16] R. Chodura, in *Physics of Plasma Wall Interactions in Controlled Fusion*, edited by D. E. Post and R. Behrisch (Plenum, New York, 1986), p. 99.
[17] G. S. Kino and E. K. Shaw, Phys. Fluids **9**, 587 (1966).
[18] B. A. Trubnikov, *Reviews of Plasma Physics,* edited by M. A. Leontovich (Consultants Bureau, New York, 1965), p. 105.
[19] P. L. Bhatnagar, E. P. Gross, and M. Krook, Phys. Rev. **94**, 511 (1954).
[20] E. M. Lifshitz and L. P. Pitaevskii, *Physical Kinetics* (Pergamon, Oxford, 1981), Chap. 6, p. 168.
[21] D. Bohm, in *The Characteristics of Electrical Discharge in Magnetic Fields,* edited by A. Guthrie and R. K. Wakerling (McGraw-Hill, New York, 1949), Chap. 3, p. 77.